Cell

Structural Insights into RNA-Dependent Ring Closure and ATPase Activation by the Rho Termination Factor

Emmanuel Skordalakes[1] and James M. Berger[1,*]
[1] Department of Molecular and Cell Biology, University of California, Berkeley, 327B Hildebrand Hall #3206, Berkeley, CA 94720, USA
*Contact: jmberger@berkeley.edu
DOI 10.1016/j.cell.2006.08.051

SUMMARY

Hexameric helicases and translocases are required for numerous essential nucleic-acid transactions. To better understand the mechanisms by which these enzymes recognize target substrates and use nucleotide hydrolysis to power molecular movement, we have determined the structure of the Rho transcription termination factor, a hexameric RNA/DNA helicase, with single-stranded RNA bound to the motor domains of the protein. The structure reveals a closed-ring "trimer of dimers" conformation for the hexamer that contains an unanticipated arrangement of conserved loops required for nucleic-acid translocation. RNA extends across a shallow intersubunit channel formed by conserved amino acids required for RNA-stimulated ATP hydrolysis and translocation and directly contacts a conserved lysine, just upstream of the catalytic GKT triad, in the phosphate-binding (P loop) motif of the ATP-binding pocket. The structure explains the molecular effects of numerous mutations and provides new insights into the links between substrate recognition, ATP turnover, and coordinated strand movement.

INTRODUCTION

Oligomeric, ring-shaped ATPases are abundant in nature and regulate many essential cellular processes. Hexameric helicases and translocases, which comprise a subset of these enzymes, serve as molecular motors that hydrolyze nucleoside triphosphates (NTPs) to facilitate nucleic-acid movement and/or unwinding for controlling replication, chromosome packaging, and other events (Bird et al., 1998; Delagoutte and von Hippel, 2003; Patel and Picha, 2000; von Hippel and Delagoutte, 2001). All hexameric helicases and translocases identified to date are built upon a common structural building block, the RecA or AAA+ domain, both of which fall within a broad P loop superfamily of NTPases (Bird et al., 1998; Iyer et al., 2004; Patel and Picha, 2000).

The Rho transcription termination factor is a RecA-type, ring-shaped hexameric helicase that regulates gene expression in bacteria (Richardson, 2002). Rho specifically associates with *R*ho *ut*ilization (*rut*) loci in particular nascent mRNAs through a primary RNA-binding site contained within its N-terminal domain (Alifano et al., 1991; Morgan et al., 1985). RNA binding to the primary site triggers ring opening (Jeong et al., 2004; Skordalakes and Berger, 2003; Yu et al., 2000), which allows a single strand of mRNA to enter the interior of the particle and associate with a secondary RNA-binding site formed by two signature sequence motifs (the Q and R loops) located in its RecA fold (Burgess and Richardson, 2001; Hingorani and Patel, 1993; Jezewska et al., 1996; Miwa et al., 1995; Wei and Richardson, 2001; Yu et al., 1996). RNA binding to the secondary site is thought to stimulate ring closure, an event that facilitates the formation of a catalytically competent ATPase and turns Rho into an active translocase (Gogol et al., 1991; Yu et al., 2000). The mechanisms by which RNA/motor domain contacts help regulate ring closing and activate Rho's ATPase remain unclear.

During translocation, Rho is thought to successively fire its ATPase sites in a sequential manner as it moves along a nucleic-acid track (Kim and Patel, 1999; Stitt and Xu, 1998). This mode of action is similar to that proposed for several other hexameric helicase/translocase proteins, including the DnaB replication fork helicase, the bacteriophage T7gp4 helicase/primase, and the phage ϕ12 P4 RNA packaging protein (Bujalowski and Jezewska, 2000; Hingorani et al., 1997; Lisal and Tuma, 2005; Mancini et al., 2004). Energy derived from ATP hydrolysis drives nucleic-acid movement and duplex unwinding, a process coordinated in part by structural elements equivalent to Rho's Q loop (also known as L2 loops), which protrude from the ATPase domain into the center of the hexameric ring (Gai et al., 2004; Mancini et al., 2004; Singleton et al., 2000). The L2 loops of T7gp4 and ϕ12 P4, as well as those of the AAA+-type SV40 large tumor

antigen, have been directly observed to lever up and down the axis of the helicase ring in response to the nucleotide status of their adjoining ATPase active site (Gai et al., 2004; Mancini et al., 2004; Singleton et al., 2000), a conformational change that likely manifests the power stroke to drive nucleic-acid substrates through the helicase ring. It is unknown in Rho whether the coupling between ATP turnover and nucleic-acid movement is entirely allosteric, with chemical events at the ATPase site linked to RNA/Q loop movement at a distance through a proteinaceous relay network. It is similarly unclear whether RNA remains associated with the same subunit throughout translocation, whether it is coordinated by multiple subunits simultaneously, or whether it is actively transferred from one subunit to another.

To address these issues, we have determined the structure of *E. coli* Rho in complex with a 30 nucleotide RNA substrate. The structure reveals a closed-ring, 3-fold-symmetric ("trimer of dimers") conformation, consistent with earlier symmetry models derived from prior biochemical studies (Geiselmann et al., 1992a, 1992b; Horiguchi et al., 1997; Kim and Patel, 1999; Stitt, 2001; Xu et al., 2003). The principle translocation element of Rho, the Q loop, adopts two markedly distinct configurations that alternate between adjacent protomers around the ring in a manner not seen previously in other hexameric helicase/translocase structures. RNA binds in a shallow channel formed by the interface of two adjacent ATPase domains, where it contacts Rho's second translocation element, the R loop. Unexpectedly, RNA interacts with a conserved lysine located within the Walker A motif and adjacent to the catalytic glycine-lysine-threonine (GKT) triad. These findings demonstrate that RNA directly communicates with the ATPase active site of Rho's motor domains and provide a molecular rationale for the behavior of numerous ATPase- and translocation-defective mutants. Our results afford new insights into how nucleic-acid binding stimulates ring closure and suggest that RNA may be directly exchanged from one subunit to another by a concerted "handoff" mechanism.

RESULTS

Structure Determination

We used limited proteolysis to isolate a new variant of *E. coli* Rho that would crystallize with long RNAs (20- to 30-mers) capable of stimulating the helicase's ATPase activity (see the Supplemental Experimental Procedures and Figure S1 in the Supplemental Data available with this article online). Mass spectrometry of harvested crystals revealed the presence of a Rho fragment missing only the C-terminal 8 amino acids of the protein (Rho_{411}), which were poorly ordered in an earlier structure of Rho (Skordalakes and Berger, 2003). A gene encoding this construct (Rho_{411}) was recombinantly expressed to optimize crystal quality and for use in subsequent biochemical studies. The new crystal form belongs to the cubic space group I432 and contains one dimer per asymmetric unit that, due to crystallographic symmetry, forms part of a hexameric particle along with two other subunit pairs. Initial phases were calculated by molecular replacement using individual subdomains of the *E. coli* Rho monomer (PDB ID code 1PVO) as a search model. These phases were used to find heavy metal sites in gadolinium (Gd) and brominated-RNA derivatives (Table 1); electron density obtained by anomalous diffraction experiments (Gd-MAD and Br-SAD) helped validate the placement of individual domains and the main-chain trace as determined by molecular replacement and was used to visualize and confirm the location of the RNA bound to Rho's secondary RNA-binding site (Experimental Procedures). Electron density was evident for residues 31–354 of both Rho protomers and for three RNA segments. The final model has been refined to 3.5 Å resolution and shows good stereochemistry (Table 1).

The Rho Protomer

Each Rho subunit consists of two distinct functional domains (Figure 1A) (Richardson, 1996; Seifried et al., 1991). The N-terminal domain contains an oligonucleotide/oligosaccharide-binding (OB) fold that binds cytosine-rich RNAs and constitutes Rho's primary RNA-binding site (Allison et al., 1998; Bogden et al., 1999; Richardson, 1996). The C-terminal domain adopts a RecA-type fold, which is most structurally similar to the mitochondrial F_1 ATPase C-terminal domain, and contains Rho's nucleotide and secondary RNA-binding sites (Abrahams et al., 1994; Bird et al., 1998; Miwa et al., 1995; Skordalakes and Berger, 2003).

Comparison of the two Rho protomers in the asymmetric unit (labeled A and B to distinguish between them) shows that their structures are highly similar (Cα rmsd = 0.69 Å for all amino acids). There are, however, significant differences between the protomer structures observed here and those of full-length Rho determined previously (Skordalakes and Berger, 2003) (Figure 1B). One is that the N-terminal domain is rotated by $\sim$7° counterclockwise about the top of the C-terminal domain. This movement is concomitant with a loss of interpretable electron density for the first 30 amino acids at the extreme N terminus, a highly variable and typically Arg/Gly-rich region of Rho orthologs. Another difference is that the last 65 amino acids of the C-terminal domain are disordered and have been displaced in part by residues from the connector loop that links the N- and C-terminal domains. This change is accompanied by an $\sim$40° rotation of helix α6, which lies at the end of the connector, from its position seen previously. The physical basis for and consequences of these changes are discussed in greater detail in the Supplemental Experimental Procedures and Figures S1 and S2.

The Rho Hexamer

Within our crystals, three dimers are crystallographically related to one another to form an intact, closed-ring Rho hexamer that is 3-fold symmetric (Figure 2A). Unlike the

Table 1. Data Collection Statistics

Data Set	Native	Gd-MAD		5BrU
Space group	I432	I432	I432	I432
Unit cell a (Å)	257.1	256.9	256.9	256.6
Wavelength	1.11 Å	1.6000 Å (low E)	1.7107 Å (peak)	0.9202 Å (peak)
Resolution range (Å)	50–3.5	50–4.6	50–4.6	50–6.15
Redundancy (high-resolution bin)	3.3 (2.7)	5.3 (4.3)	5.1 (4.1)	6 (6.4)
Completeness (%)	91.9 (86.9)	98.3 (97.3)	99.5 (99.3)	99.9 (99.9)
I/σ	8.3 (1.7)	7.2 (3.1)	7.3 (2.8)	5.5 (1.4)
R_{merge} (%)	8.9 (53.3)	15.5 (49.4)	16.3 (57.3)	14.0 (58.3)
Figure of merit[a]		0.42 (50–4.6 Å)		
Refinement				
Resolution	20–3.5 Å			
Reflections	15,818			
Working set	15,011			
Test set	807			
Wilson B	122			
Average B factor, protein	117			
Average B factor, RNA	127			
Rmsd bonds (Å)	0.006			
Rmsd angles (°)	0.966			
R_{work} (%)[b]	29.5			
R_{free} (%)[c]	32.8			
Ramachandran				
Favored	86			
Additional	13.3			
Generous	0.7			
Disallowed	0			
Number of atoms				
Protein	5,044			
RNA	180			
Ions	10			

[a] Figure of merit = $<|\Sigma P(\alpha)e^{i\alpha}/\Sigma|P(\alpha)|>$, where α is the phase and $P(\alpha)$ is the phase probability distribution.
[b] $R_{work} = \Sigma\Sigma|F_o - F_c|/\Sigma F_o$
[c] R_{free} was calculated as R_{work} using 5% of the data not included in refinement.

left-handed, spiral lock-washer architecture displayed by the open-ring state of Rho (Skordalakes and Berger, 2003), the closed-ring structure is flat. The transition from the open-ring state to closed-ring state arises from a concerted 15° inward rotation of each subunit about an axis perpendicular to the ring axis, leading to a ~7.5 Å shift with respect to its neighboring subunit (Figure 2; Movie S1). The mechanism of ring closure used by Rho is different from that observed for the conversion of T7gp4 from a right-handed helical filament to a closed-ring hexamer (Sawaya et al., 1999; Singleton et al., 2000); however, the locus of movement is similar, arising from conserved structural elements that form an intersubunit contact point in oligomeric RecA folds (helix α11 of one protomer and the β7/α8 and β8/α9 loops of its neighboring subunit in Rho) (Figure 1A). The Rho ring-closing motion further coincides with an inward rotation of every B protomer that orients these three subunits slightly closer to the center of the ring than their A subunit counterparts. It is noteworthy that these motions, coupled with the added rotation of the N-terminal OB domain with respect to the C-terminal RecA fold, position the primary

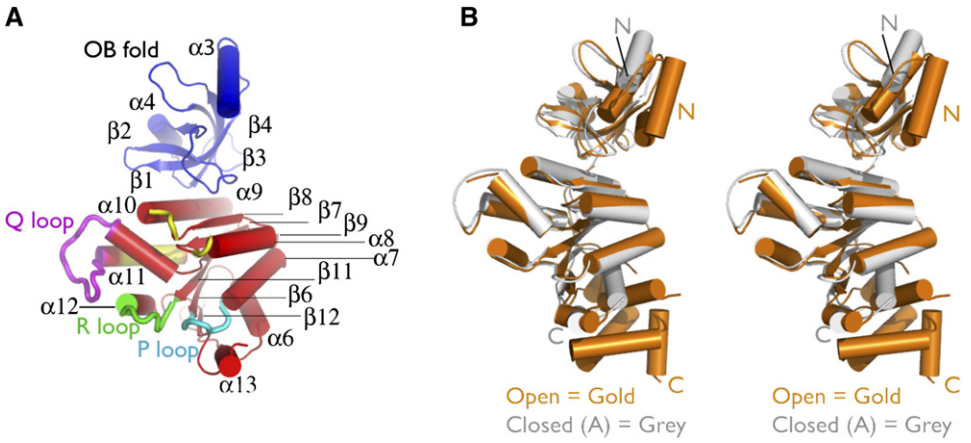

Figure 1. Rho Protomer Structure

(A) Structure and topology of the closed-ring Rho protomer. The RecA domain is shown in red, and the OB fold is shown in blue. Translocation (Q and R) and catalytic (P) loops are highlighted in magenta, green, and cyan, respectively. Regions colored yellow indicate subunit-subunit contact points that hinge with respect to each other between open- and closed-ring Rho states (see Figure 2). Secondary structural elements are labeled (Skordalakes and Berger, 2003).

(B) Overlay of protomers from the open-ring (gold, PDB ID code 1PVO) and closed-ring (gray) Rho conformations. N and C termini are labeled.

RNA-binding sites 5.5 Å closer to the interior of the hexamer than observed in the open-ring Rho conformation. In contrast to the open-ring structure, no contacts were observed between the N-terminal domains in the closed-ring structure.

Rho's ATP-Binding Pocket

Each ATP-binding pocket of Rho is formed at the interface between two adjacent C-terminal domains and contains the Walker A and B signature sequence motifs common to all RecA-type ATPases. Despite requiring nucleotides (AMPPNP and ADP) for crystallization, no electron density was evident for these molecules in the ATP-binding site. Instead, density consistent with the presence of a sulfate ion appears to occupy the P loop region of the Walker A motif (Figure S3A). Prior structural studies of *E. coli* Rho have shown that the side chains of two conserved amino acids, Met186 and Phe355, are responsible for

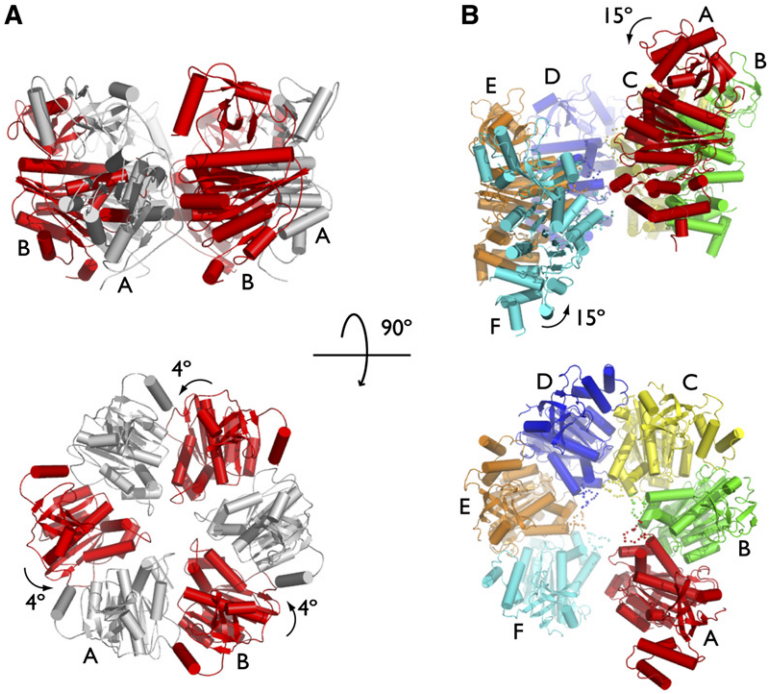

Figure 2. Structural Transitions in the Rho Hexamer

(A) Closed-ring conformation shown in edge-on (upper panel) and top-down views (lower panel). Equivalent A and B subunits are colored gray and red, respectively. Arrows mark the inward rock of the B subunit with respect to A.

(B) Open-ring conformation. Each subunit is differently colored and labeled. Perspectives are the same as in (A). Numbers represent the degree and arrows the direction of rotational shift of one subunit with respect to its neighbors between the open- and closed-ring structural states.

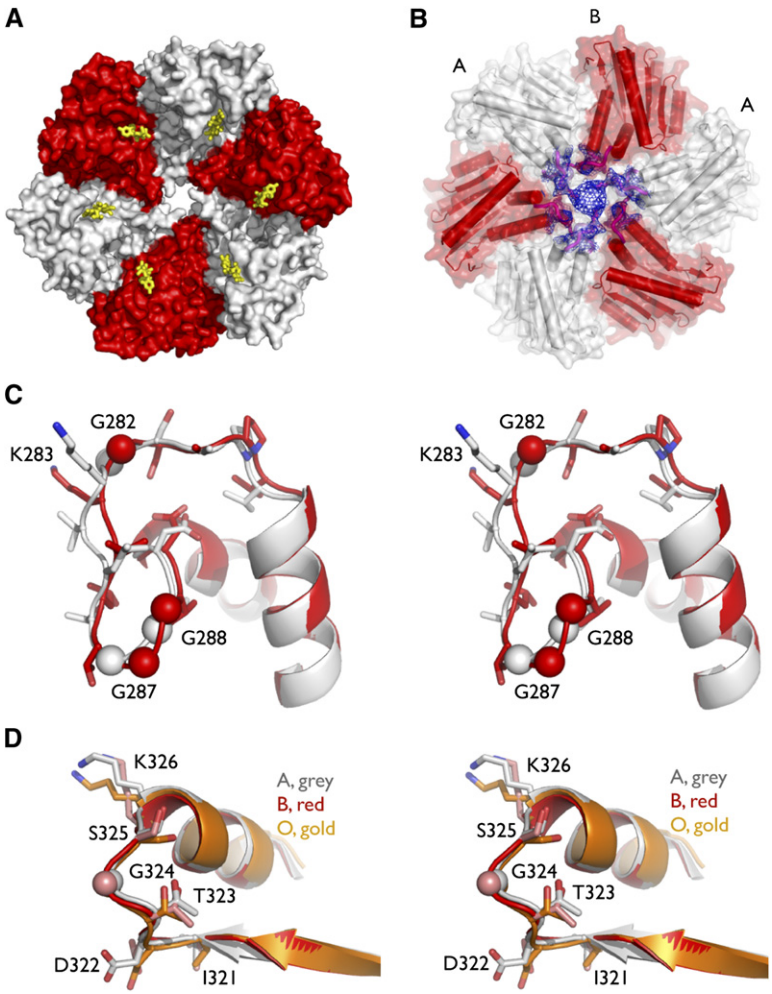

Figure 3. Primary and Secondary RNA-Binding Sites of Rho

(A) Surface representation of the closed-ring Rho hexamer (top-down view). RNA bound to primary RNA-binding sites is shown as yellow sticks. The Rho A and B subunits are alternately colored gray and red.

(B) Top-down view of the Rho hexamer showing two distinct orientations of Lys283 (spheres) within the Q loops (magenta). The N-terminal domains have been removed for clarity. Experimental electron density (Gd phased, 1.0σ above the mean) is shown around the lysines, and the interior of the Rho ring is shown as a blue mesh. Strong density is evident in the central hole of the hexamer.

(C) Stereogram overlaying Q loops from protomers A (gray) and B (red) and showing their distinct conformations.

(D) Stereogram overlaying R loops from protomers A (gray) and B (red) of closed-ring Rho and protomer A (gold) of the open-ring conformation.

sandwiching the adenine moiety of bound nucleotide. Since Phe355 lies within the C-terminal region of Rho that is disordered in this crystal form, and since Rho_{411} retains length-dependent RNA-stimulated ATPase activity (Figure S1), it is likely that nucleotide is unable to remain stably associated with the protein when confronted with the high sulfate concentrations (~1.0 M) in the crystallization solution.

Structural comparisons of A/B and B/A subunit junctions show that the separation between protomers differs by less than a few angstroms around the region comprising the ATP-binding site (Figure S3B). Superpositions of either RecA dimer from Rho with homologous F_1 ATPase interfaces imaged in different nucleotide-binding states ("tight," "loose," and "open"; Abrahams et al., 1994) indicate that the spatial configuration of Rho's ATP-binding pockets are equally similar to all three F_1 conformations (Cα rmsd = 1.9 Å). It thus appears that Rho's ATPase domains have adopted an intermediate conformation between those of the ATP-free and ATP-bound subunit interfaces in F_1, an organization that may arise from sulfate binding to all six protomers.

Rho's Primary and Secondary RNA-Binding Sites

The primary RNA-binding sites of Rho have been shown previously to bind a dinucleotide segment in a network of contacts that explains the preference of the helicase for pyrimidines, particularly cytosine (Bogden et al., 1999; Chen et al., 1986; Galluppi and Richardson, 1980; McSwiggen et al., 1988; Modrak and Richardson, 1994). Electron density is evident for a pyrimidine dinucleotide in the OB folds of both subunits in the closed-ring state, recapitulating OB-fold/RNA interactions similar to those seen in other Rho structures. Like its open-ring counterpart, the closed-ring Rho particle orients the RNA-binding clefts of each N-terminal domain toward the central hole of the ring (Figure 3A), placing the nucleic-acid 3′ end in proximity to the secondary RNA-binding site (Skordalakes and Berger, 2003).

Rho's secondary RNA-binding site is formed by two structural motifs, known historically as Q and R loops (Miwa et al., 1995). The Q loops lie in the RecA fold between helices α10 and α11 (Figure 1A) and together form the narrowest constriction within the central channel of the ring (Figure 3B). In the open-ring Rho structure, the

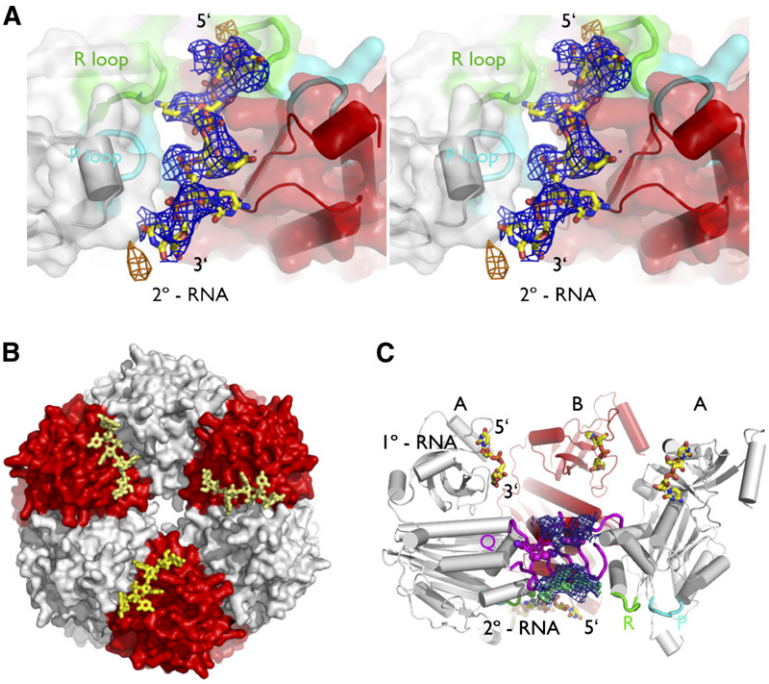

Figure 4. RNA Binds to the ATPase Domains of Rho

(A) Stereoview of the Rho C-terminal domain (transparent surface with cartoon) showing experimentally observed electron density (F_{obs}, α_{DM}, 1σ contour in blue) from Gd-MAD-phased data for ssRNA bound in a channel formed at the A/B subunit interface. Anomalous difference density peaks (3σ contour) from a brominated RNA derivative are shown in gold. Subunits A and B are colored gray and red, respectively; R and P loop regions are highlighted green and cyan, respectively.

(B) Surface representation of the closed-ring Rho hexamer (bottom-up view) showing globally where RNA (yellow sticks) binds to the protein's RecA folds. Although Rho is expected to bind only one strand of RNA at a time, the hexamer axis is coincident with a crystallographic 3-fold axis. As a consequence, electron density is evident at all three A/B interfaces, and three RNA chains ("principal" ligand at bottom; two crystallographically related molecules at top) are depicted for accuracy. See Experimental Procedures for details.

(C) Cross-section through the Rho ring. The view shows three of Rho's six subunits, along with experimental MAD density (1σ and 2.5σ contour, blue and green mesh, respectively) for the region. The electron density is present in stacks above and below the aperture formed by Lys283 of the Q loops. The P, Q, and R loops are colored cyan, magenta, and green, respectively; Lys283 is shown as magenta sticks. RNA bound to each of the OB folds (upper sticks) and to the A/B RecA domain interface (lower sticks) is shown in yellow CPK coloring, with 5′ and 3′ termini labeled. For a single RNA, the 3′ end of an upper RNA chain would extend downward, pass through the central Rho channel and between the Q loops, and connect with the 5′ end of the lower RNA segment bound to the motor domains.

Q loops are only partly ordered in all six subunits (Skordalakes and Berger, 2003). By contrast, clear electron density is observed for the Q loops in the closed-ring state. Each Q loop forms a hairpin-like structure with a well-defined configuration. The conformations of the Q loops, however, differ strikingly between the two protomers in the asymmetric unit (Figure 3C): In protomer A, the side chains of the Q loop (particularly Lys283) extend into the center of the ring (Figure 3B), whereas the side chains of the B subunit Q loop are predominantly buried, leaving exposed a relatively flat and nonpolar backbone surface. The conformational change in this region results in part from a remodeling of backbone torsion angles around two invariant glycine residues (Gly282 and Gly287) that flank the two ends of the loop (Table S1 and Movie S2).

In contrast to the Q loops, the R loops in the closed-ring structure adopt a conformation highly similar to each other (Figure 3D). Each R loop consists of a short rigid extension that lies between β11 and α12 and is located both between and in close proximity to the Q and P loops (Figure 1A). The location of the R loop is consistent with biochemical data showing that this motif functions to couple ATP turnover with RNA binding (Engel and Richardson, 1984; Kim and Patel, 2001; Richardson and Conaway, 1980; Shigesada and Wu, 1980). Structural comparisons show that the conformation of the R loop remains constant in both open-ring and closed-ring states (Cα rmsd = 0.49 Å; Figure 3D), indicating that this region does not undergo any internal rearrangements as Rho transitions between these two hexamer conformations.

RNA Bridges the R Loop and ATPase Site

Inspection of initial molecular replacement maps showed weak electron density localized to the interface between the RecA domains of the A/B subunit pair. No density was observed at the corresponding B/A interface. The connectivity and featuredness of the density were dramatically improved in medium-resolution (4.6 Å), MAD-phased maps obtained from a Gd-derivatized crystal (Table 1). Model building revealed that a pentanucleotide RNA segment fit well into this region (Figure 4A). Data collected from a brominated RNA derivative further validated chain placement (Experimental Procedures).

The backbone of bound RNA runs along the middle of a shallow channel where the R and P loops are located (Figures 4A and 4B). Bases extend away from the backbone in roughly opposing directions, contacting the side chains of a number of residues from both protomers (Figures 5A and 5B). RNA interacts with the R loops of both protomers through nucleotides rU_1 and rC_2 at the 5′ end of the nucleic acid: The sugar 2′OH of rU_1 is liganded by the side chain of Asp_B322 (where the subscripted B denotes the side chain from protomer B), while the base of rC_2 associates with the side chains of Lys_B336 and Asp_A322. Contacts between rU_3 and the protein are mediated by the imidazole moiety of His_B344, which hydrogen

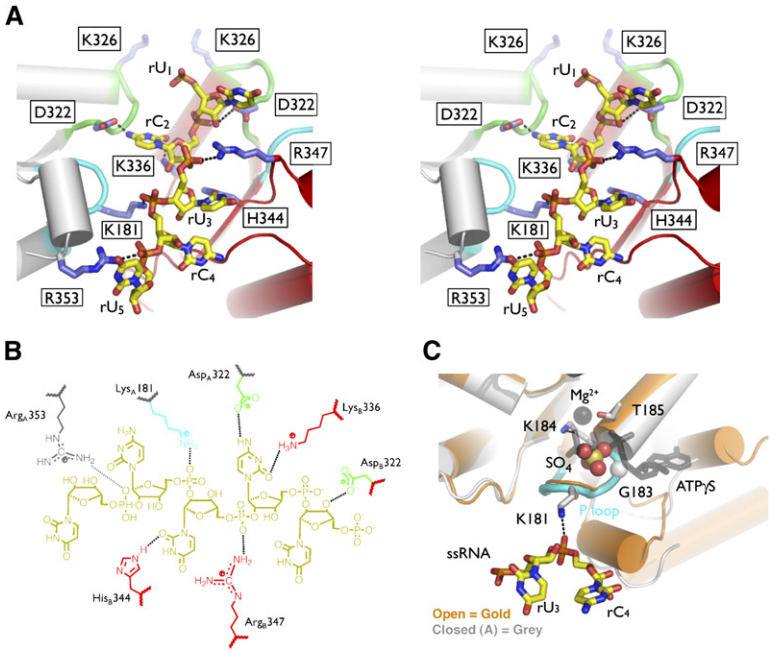

Figure 5. Rho-RNA Interactions

(A) Stereogram of protein/RNA contacts. Q, R, and P loops are shown in magenta, green, and cyan respectively. The A and B subunits are colored gray and red, while RNA is shown as yellow sticks. Labels for amino acids that affect enzyme activity when mutated are boxed.

(B) Schematic of Rho-RNA contacts, colored as in (A).

(C) Superposition of the ATP-binding pocket of closed-ring Rho (gray) with that of nucleotide-bound Rho (gold; PDB ID code 1XPU). The location of the lysine (K184) in the catalytic GKT triad and the P loop lysine (K181) that coordinates the RNA are shown. The sulfate ion modeled in the closed-ring state and the nucleotide bound to the open-ring state are shown as colored spheres and transparent black sticks, respectively (see also Figure S4).

bonds the base, and by the guanidinium group of Arg_B347, which forms a salt bridge with the phosphodiester backbone of the same nucleotide. Unexpectedly, the phosphate of rC_4 is seen to directly contact the P loop of protomer A by forming an ion pair with the side chain of Lys_A181; this amino acid lies just upstream of the catalytic Walker A lysine (Lys184) of the GKT motif, thus linking the ATPase active site to the RNA substrate (Figure 5C; Figure S4). Finally, the phosphate of rU_5 appears to associate with the side chain of Arg_A353, although the poor quality of electron density and high B factors for this region make this assignment somewhat tentative. It is notable that all of the side chain-RNA contacts observed here are mediated by highly conserved or invariant surface-exposed amino acids. The directionality of the RNA also agrees with the known translocation polarity of Rho, placing the 5′ end of the single strand in proximity to the Q loops (and closer to the N-terminal domains) and the 3′ end on the far side of the C-terminal domain (Figure 4).

In contrast to the regions around the P and R loops, no interpretable electron density was observed for RNA bound to the Q loops. Since the 3-fold axis of the Rho ring is coincident with a 3-fold crystallographic symmetry axis, this happenstance most likely derives from positional averaging of the RNA signal as the chain passes through the central channel of the hexamer. Consistent with this reasoning, strong stacks of experimental electron density (from Gd-MAD-phased data) that thread between the Q loops and do not correspond to the polypeptide chain of Rho are evident within the hole of the Rho ring (Figure 3B and Figure 4C). Our observations that the long RNAs used to produce this crystal form also stimulate Rho's ATPase activity (Figure S1A) and that buildable density is present in the R loop regions leading up to the Q loops (Figure 4A) further indicate that, although not modelable, RNA is nevertheless bound to the Rho interior.

Observed Rho-RNA Interactions Correlate with Existing Mutational Data

To date, a large number of Rho mutants that affect RNA binding, RNA-stimulated ATP hydrolysis, and Rho's ability to terminate transcription have been isolated (Dombroski et al., 1988; Miwa et al., 1995; Xu et al., 2002). The closed-ring Rho structure shows that a number of these mutations colocalize to the RNA-binding channel between adjacent RecA domains and alter residues that contact the nucleic-acid segment (Figure 5A). These associations serve as corroborative evidence for our interpretation of the electron density in this region and in turn provide a molecular explanation for the biological and biochemical effects of specific alterations.

For example, the substitutions Lys181Gln, Lys336Ala, Arg347Gly, and Arg353Ala all show decreased turnover rate for poly(C)-dependent ATP hydrolysis, a diminished ability to terminate transcription compared to wild-type Rho, and (with the exception of Lys181Gln) a decrease in RNA-binding affinity (Dombroski et al., 1988; Miwa et al., 1995; Xu et al., 2002). All four amino acids are highly conserved and hydrogen bond to specific bases and phosphodiester linkages in the RNA (Figure 5A). Lys181 is particularly noteworthy because it directly associates with the phosphate of bound RNA and is part of the P loop of Rho's ATPase site (Figure 5C). As a consequence of these associations, the loss of function observed from mutating any of these residues likely arises from simple disruption of key contacts with RNA substrates.

Other alterations can be similarly reconciled with our structural data. For example, the His344Arg mutant shows

increased affinity for RNA compared to wild-type Rho and correlates with a "super-Rho" phenotype that overterminates transcription (Miwa et al., 1995). Modeling studies indicate that replacement of His344 (which makes direct base contacts to RNA) with the longer and positively charged side chain of arginine could permit formation of a new salt bridge with the nucleic-acid phosphodiester backbone, perhaps helping to stabilize Rho-RNA interactions. The Lys283Glu mutation, which abrogates the ability of poly(rC) to stimulate Rho's ATPase activity (Xu et al., 2002), is similarly interesting. Lys283 is part of the Q loop and, together with several symmetry-related counterparts, forms a collar of positively charged residues at the center of the Rho ring (Figure 3B). Substitution of this lysine with glutamate could be expected to disrupt appropriate interactions of this region with negatively charged RNA substrates.

DISCUSSION

RNA-Dependent Ring Closure

The first high-resolution structure of the Rho hexamer was determined with RNA bound only to its N-terminal, primary RNA-binding sites (Skordalakes and Berger, 2003). This model exhibited an open-ring conformation thought to reflect a possible RNA-loading state; however, several lines of evidence indicated that, when bound to an extended RNA chain, Rho would subsequently convert into an active, closed-ring form (Gogol et al., 1991; Richardson, 1982; Yu et al., 2000). Interactions with the secondary RNA-binding site of Rho, which are necessary to facilitate ATP turnover, have been proposed to drive this transition (Seifried et al., 1992).

The closed-ring Rho structure demonstrates the remarkable structural flexibility that allows the enzyme to transition between open-ring and closed-ring configurations (Figure 2; Movie S1). Comparison of the two Rho structures reveals that simple but concerted rotational changes between each of the six subunits are all that is needed to convert from a conformation favorable to RNA loading to one that is used for translocation (Figure 1). These findings provide a structural framework for the design of experiments to probe the mechanics of this event in Rho, as well as to explore whether other families of toroidal helicases that load onto nucleic-acid substrates as intact assemblies (e.g., DnaB or MCM) undergo similar types of subunit rearrangements.

RNA-Dependent Activation of Rho ATPase

An unanticipated discovery arising from this work is that Rho can bind RNA in a channel formed at the interface between RecA subunits that spans the ATP-binding site (Figure 4). Significantly, structural elements used for ATP binding and hydrolysis (such as the P loop) also are seen to interact directly with nucleic-acid substrate (Figure 5C). For Rho, the amino acid that mediates this contact, Lys181, is always lysine or arginine in different Rho orthologs. Given that mutation of this residue diminishes the ability of RNA to stimulate Rho's ATPase activity (Dombroski et al., 1988), our results indicate that RNA binding may directly influence the state of the ATPase site to regulate hydrolysis. Interestingly, although amino acids within the Walker A element (but upstream of the catalytic GKT triad) vary greatly between oligomeric helicase/translocase families, these enzymes typically contain one or more bulky amino acids in this traditionally glycine-rich P loop motif (e.g., Lys131 in ϕ12 P4 or Met316 in T7gp4). It will be important to determine whether the direct nucleic acid/ATPase site interactions seen in Rho are actually part of a universal mechanism employed by distantly related oligomeric RecA-family helicases to help couple substrate binding with nucleotide turnover.

Control of Translocation-Loop Position

Understanding how Rho and other helicase/translocase proteins move along nucleic-acid segments remains an outstanding question. Although the closed-ring structure of Rho does not have nucleotide bound to its ATPase sites, it does exhibit structural features consistent with L2 loop lever models for translocation (Gai et al., 2004; Mancini et al., 2004; Singleton et al., 2000). For example, between the A and B subunits, not only does Lys283 change from an exposed to a buried state, its side chain also rises along the ring axis by ~2 Å (data not shown). Similarities between Rho and the F_1 ATPase provide additional clues to the power stroke. Given the sequence and structural homology of these two proteins, one would expect Rho's ATP-binding pocket to resemble the "tight" or activated ATP-binding site of F_1 when bound to nucleotide. Modeling this subunit/subunit conformation on Rho shows that nucleotide binding appears to push the Q loop of the A subunit upward by about 4 Å (Figure 6A). Both motions are consistent with translocation models that invoke longitudinal Q loop movements to pull RNA through the center of the ring.

A Directed Subunit-Handoff Model for RNA Exchange

Understanding whether and how nucleic acids are actively passed from one subunit to another during translocation is a similarly pressing issue. The two conformations of Q loops observed in our crystal structure provide new clues to this process in Rho. Except for an invariant basic residue (Lys283), the Q loop is composed exclusively of serine and β-branched amino acids (SGKVLTGGV) and contains three invariant glycines that flank both ends of the motif. An inspection of main-chain torsion angles for residues within the Q loop shows that ϕ/ψ isomerization events for several amino acids help accommodate the switch between the two conformations observed in the closed-ring crystal structure (Figure 3C; Table S1 and Movie S2).

The Q loop, which is nearly invariant among Rho homologs, is also conserved with the catalytically active β subunit of the F_1 ATPase. When viewed from the top, the alternating conformations of the Q loops impart a distinct counterclockwise directionality to Rho that is strikingly similar to F_1 (Figure 3B and Figure 6B). Moreover, when

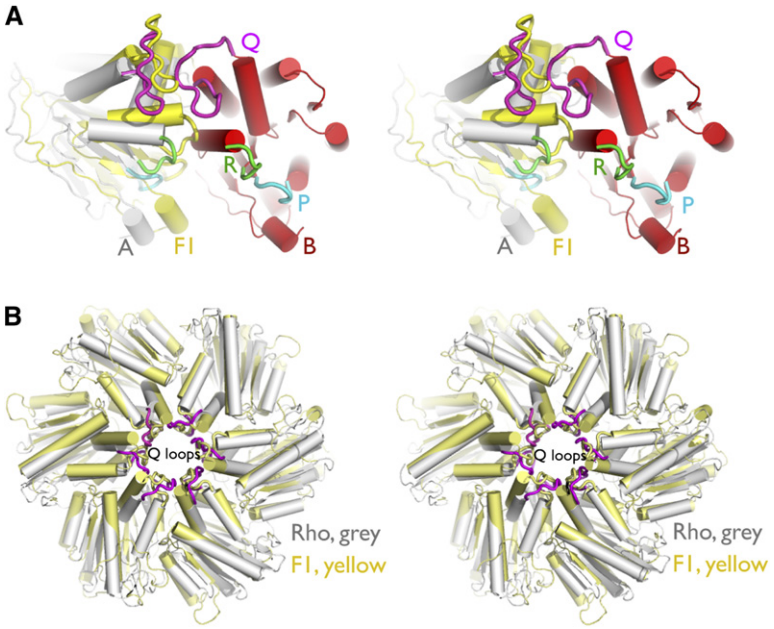

Figure 6. Rho/F_1 ATPase Comparisons

(A) ATPase domain orientations in a nucleotide-bound F_1 active site compared to Rho. Stereogram shows the Rho ring from the inside looking out. Adjoining A and B subunits in closed-ring Rho are colored gray and red. Using adjacent β/α subunits from F_1 bound to AMPPNP as a guide (PDB ID code 1BMF), a model for an ATP-bound conformation of Rho was generated and superposed with the closed-ring configuration. The process indicates that the F_1 α protomer (yellow) is rocked upward by ~14° with respect to the F_1 β subunit as compared to the equivalent A/B subunit orientation seen in Rho. A corresponding movement in Rho upon ATP binding to subunit B would push the Q loop region above that seen in the closed-ring structure for subunit A by ~4 Å.

(B) Stereogram overlaying the RecA folds from closed-ring Rho (gray) with those of F_1 bound to AMPPNP and ADP (yellow) (Abrahams et al., 1994). View is from the top (as in Figure 2A).

the RecA folds of the hexamers are aligned, the Q loops of Rho superpose exceedingly well with corresponding regions of the F_1 β subunits (Cα rmsd = 1.8 Å). F_1 is notable among hexameric ATPases in that it is the only ATPase unequivocally shown to sequentially fire its active ATPase sites about the ring as it spins an internal shaft element (Noji et al., 1997). Given Rho's close sequence homology to F_1, the high degree of structural and conformational similarity observed here strongly reinforces models positing that Rho will utilize a rotary mechanism (Geiselmann and von Hippel, 1992; Geiselmann et al., 1993; Kim and Patel, 1999; Stitt, 2001; Stitt and Xu, 1998; Xu et al., 2003).

Taken together, these findings add several new dimensions to our understanding of Rho function. The relative spatial configuration between functionally important residues in the Q loops, which together enclose an interior space that can accommodate a single mononucleotide of an extended RNA chain (Figure 7A), suggest that RNA binding to the hole of the hexamer helps set up and sterically reinforce conformations seen here for this region. The observation that RNA interacts directly with the P loop (Figure 5) and that a conserved amino acid mediating this contact (Lys181) potentiates RNA-stimulated ATP turnover (Dombroski et al., 1988) suggests that only a single ATPase site—the one associated with RNA—fires at any given moment within the hexamer. The R loops, which are critical for Rho function, are rigidly fixed in all structures determined to date (Figure 3D) and do not appear to act in an allosteric manner. These elements appear instead to serve as "guideposts" that help direct RNA from its associated Q loop into an intersubunit channel where it can contact the ATPase site (Figure 5A).

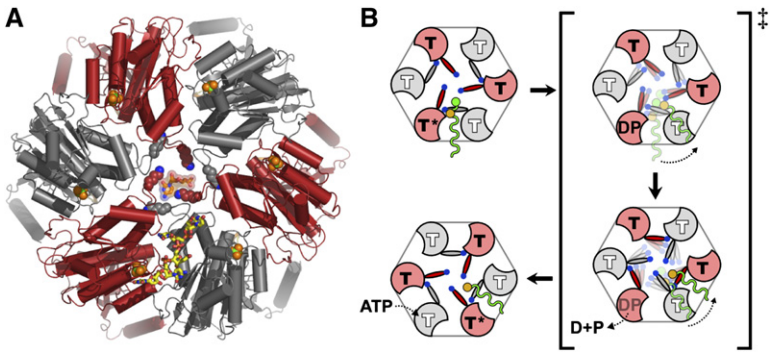

Figure 7. Model for Q Loop Reorientation and RNA Handoff

(A) The central channel of Rho can sterically accommodate one strand, but not two strands, of RNA. View shows a single RNA chain (yellow sticks) bound to a pair of motor domains in the hexamer. A sulfate ion (black spheres) marks the P loop of the ATPase site. Q loop lysine side chains (Lys283) are depicted as red and gray spheres with blue ζ-nitrogens. The Lys283 conformations observed here can accommodate a single mononucleotide without clashes (modeled as orange sticks with a transparent van der Waals surface).

(B) Model for RNA handoff. Two protomers of a closed Rho ring are colored gray and red (bottom-up view). T* indicates the ATPase site primed to carry out hydrolysis by virtue of its interaction with bound RNA (wavy green line). The occupancy and catalytic status of ATP-binding sites in the rest of the hexamer are not addressed by this study; these subunits are unlabeled. ATP hydrolysis and product release at T* may produce the conformational changes coupled to drive Q loop movement and active transfer of RNA from one subunit interface to the next. Dashed arrows show the predicted direction for RNA handoff based on the flipping directionality of Lys283 (Movie S3).

Since Rho must translocate along an RNA track, the interactions we observe between the Rho motor domains and RNA must be dissociable. Subunit poisoning experiments, which have indicated that most or all of Rho's subunits need to be functional to support activity (Richardson and Ruteshouser, 1986), suggest that RNA will likely rebind to a new pair of motor domains once a translocation step has taken place. By analogy with F_1, whose ATPase sites convert between tight and loose states during nucleotide turnover, we propose that ATP-driven motions between adjacent RecA folds not only drive RNA release but may also provide a means for controlling Q loop conformation. If these transitions were to cause the side-chain configurations for this motif to alternate between the states observed here, such movements could serve to actively "hand off" RNA from one subunit to the next within the ring (Figure 7B; Movie S3).

In conclusion, we have elucidated how Rho converts to a closed conformation upon binding RNA. The cocrystal structure reveals that there is direct communication between the site of ATP turnover and nucleic-acid substrate and provides key insights into the movements and functions of a number of essential structural elements. Since all oligomeric helicases and translocases are predicated on a structurally homologous P loop NTPase fold (Iyer et al., 2004), we expect some of these findings to be universally shared between disparate enzyme families. However, as has been seen for the RecBCD helicase/nuclease complex (Singleton et al., 2004), and with oligomeric RecA/AAA+ ATPases in general, structural variations between evolutionarily related folds can dramatically alter intersubunit communication, translocation directionality, and even the mechanics that couple nucleotide turnover to nucleic-acid movement (Wang, 2004). In this context, our findings establish a number of mechanistic frameworks that will drive additional structure/function studies in Rho and related systems to help delineate these properties in the future.

EXPERIMENTAL PROCEDURES

Protein Expression and Purification

An open reading frame coding for amino acids 1–411 of *E. coli* Rho was PCR amplified and cloned into a pET27 derivative with an N-terminal hexahistidine tag. The plasmid was transformed into *E. coli* BL21(pLysS) cells and protein was overexpressed by growing cells in 2XYT media and inducing at an OD_{600} of 0.4–0.6 with 1 mM IPTG at 37°C for 3.5 hr. Cells were lysed by sonication in 25 mM Tris-HCl (pH 7.5), 10% glycerol, 0.5 M KCl on ice, and protein was purified over two successive Ni^{+}-MC columns followed by a Sephacryl S-300 (Amersham) sizing column in 25 mM Tris-HCl (pH 7.5), 10% glycerol, 0.5 M KCl. Purified protein was concentrated by ultrafiltration (Centriprep-10, Amicon) to 30 mg/ml and appeared as a monodisperse hexamer by dynamic light scattering (DynaPro, Protein Solutions). Stock protein solutions were dialyzed in 10 mM Tris-HCl (pH 7.5) and 0.5 M KCl at 4°C prior to crystallization.

Crystallization

Cocrystallization of Rho_{411} required the presence of pyrimidine-rich ssRNAs sufficiently long (20–34 nucleotides) to stimulate the ATPase activity of the full-length protein (Figure S1), as well as the nucleotides AMPPNP and ADP. Preliminary crystals diffracted to ~6 Å and required extensive optimization to diffract to 3.5 Å. Key factors included the length and sequence of the oligonucleotide and slow transfer of crystals into cryoprotectant. For optimal crystals, dialyzed protein was mixed with a 1.2-fold molar excess of $(rCU)_{15}$ ssRNA, 5 mM AMPPNP, 5 mM ADP, and 5 mM $MgCl_2$. One volume of protein was then added to one volume of crystallization solution containing 50 mM sodium cacodylate (pH 6.5), 10 mM MgOAc, 1.8 M $LiSO_4$, 2% benzamidine, and 10 mM spermine-HCl under paraffin oil at 18°C. Crystals (cubic chunks) appeared in 3–4 days and grew to ~200× 200×200 μM in 2–3 weeks. For harvesting, crystals were stepwise transferred into a cryosolution containing 25 mM sodium cacodylate (pH 6.5), 5 mM $MgCl_2$, 5 mM MgOAc, 0.98 M $LiSO_4$, 2% benzamidine, 5 mM spermine-HCl, 5 mM AMPPNP, 5 mM ADP, and 30% ethylene glycol (5% steps, 15 min/step). Stabilized crystals were then flash frozen in liquid nitrogen for diffraction measurements.

Structure Determination

Data were collected at ALS beamline 8.3.1 (MacDowell et al., 2004) and processed using ELVES (Holton and Alber, 2004). Initial phases were calculated by molecular replacement (MR) using the OB-fold and RecA-fold regions of full-length *E. coli* Rho (PDB ID code 1PVO) as a search model for PHASER (McCoy et al., 2005). Experimental maps were obtained from a gadolinium (Gd) derivative prepared by soaking the crystals with 5 mM $GdCl_3$ for 5 min; MR phases were used to locate bound Gd ions. Heavy atom parameters were refined and phases were calculated using the program MLPHARE (CCP4, 1994) followed by solvent flattening and multidomain noncrystallographic symmetry averaging using DM (Cowtan, 1994). MR and Gd-MAD maps showed electron density for ssRNA at both the primary and secondary RNA-binding sites of Rho, although the signal was stronger for the Gd data set, possibly because one Gd^{3+} ion appeared to bind to the phosphodiester backbone of the RNA itself. To further confirm the presence of RNA at the secondary RNA-binding site, Rho_{411} was cocrystallized with a 5BrU-substituted RNA substrate, $r(CUC\text{-}5BrU)_5CUC$ (Dharmacon), which contained a bromine atom at every fourth uracil nucleotide. For 5BrU-RNA/Rho cocrystals, a fluorescence scan was first used to verify the presence of brominated RNA in crystal. Data collected at the K absorption edge of the heavy atom were subsequently used to calculate anomalous difference maps, which clearly showed positive difference density at sites consistent with our RNA model (Figure 4A). All model building was carried out in O (Jones et al., 1991) followed by refinement using both CNS_SOLVE (Brunger et al., 1998) and REFMAC5 (Murshudov et al., 1997). The last few cycles of refinement were carried out with TLS restraints as implemented in REFMAC5.

It should be noted that, although Rho is thought to locally bind only one RNA chain in its motor domains, the global symmetry of the particle (trimer of dimers) permits Rho to pack in the crystal lattice in three rotational orientations. As a consequence, density for RNA within an asymmetric unit can be at most one-third of its maximal value. Accordingly, we modeled the RNA segment bound to the RecA folds with an occupancy of 0.33. Doing so allowed the average B factors for the RNA to refine to values close to those seen for the protein subunits (Table 1).

Supplemental Data

Supplemental Data include Supplemental Experimental Procedures, four figures, one table, and three movies and can be found with this article online at http://www.cell.com/cgi/content/full/127/3/553/DC1/.

ACKNOWLEDGMENTS

The authors would like to thank James Holton at Beamline 8.3.1 of the Advanced Light Source for assistance with data acquisition, David King for mass spectroscopy analyses, Tracy Young and David (Pete) Wildes for assistance with fluorescence emission and circular

dichroism data acquisition, and Allyn J. Schoeffler for assistance with ATPase assays. We thank James Keck for critical reading of the manuscript and members of the Berger lab for helpful discussions. This work was supported by the G. Harold and Leila Y. Mathers Charitable Foundation.

Received: June 5, 2006
Revised: July 25, 2006
Accepted: August 25, 2006
Published: November 2, 2006

REFERENCES

Abrahams, J.P., Leslie, A.G., Lutter, R., and Walker, J.E. (1994). Structure at 2.8 A resolution of F1-ATPase from bovine heart mitochondria. Nature *370*, 621–628.

Alifano, P., Rivellini, F., Limauro, D., Bruni, C.B., and Carlomagno, M.S. (1991). A consensus motif common to all Rho-dependent prokaryotic transcription terminators. Cell *64*, 553–563.

Allison, T.J., Wood, T.C., Briercheck, D.M., Rastinejad, F., Richardson, J.P., and Rule, G.S. (1998). Crystal structure of the RNA-binding domain from transcription termination factor rho. Nat. Struct. Biol. *5*, 352–356.

Bird, L.E., Subramanya, H.S., and Wigley, D.B. (1998). Helicases: a unifying structural theme? Curr. Opin. Struct. Biol. *8*, 14–18.

Bogden, C.E., Fass, D., Bergman, N., Nichols, M.D., and Berger, J.M. (1999). The structural basis for terminator recognition by the Rho transcription termination factor. Mol. Cell *3*, 487–493.

Brunger, A.T., Adams, P.D., Clore, G.M., DeLano, W.L., Gros, P., Grosse-Kunstleve, R.W., Jiang, J.S., Kuszewski, J., Nilges, M., Pannu, N.S., et al. (1998). Crystallography & NMR system: A new software suite for macromolecular structure determination. Acta Crystallogr. D Biol. Crystallogr. *54*, 905–921.

Bujalowski, W., and Jezewska, M.J. (2000). Kinetic mechanism of nucleotide cofactor binding to Escherichia coli replicative helicase DnaB protein. stopped-flow kinetic studies using fluorescent, ribose-, and base-modified nucleotide analogues. Biochemistry *39*, 2106–2122.

Burgess, B.R., and Richardson, J.P. (2001). RNA passes through the hole of the protein hexamer in the complex with the Escherichia coli Rho factor. J. Biol. Chem. *276*, 4182–4189.

CCP4 (Collaborative Computational Project, Number 4) (1994). The CCP4 suite: programs for protein crystallography. Acta Crystallogr. D Biol. Crystallogr. *50*, 760–763.

Chen, C.Y., Galluppi, G.R., and Richardson, J.P. (1986). Transcription termination at lambda tR1 is mediated by interaction of rho with specific single-stranded domains near the 3′ end of cro mRNA. Cell *46*, 1023–1028.

Cowtan, K. (1994). A CCP4 density modification package. Joint CCP4 ESF-EACBM Newslett. Prot. Crystallogr. *31*, 34–38.

Delagoutte, E., and von Hippel, P.H. (2003). Helicase mechanisms and the coupling of helicases within macromolecular machines. Part II: Integration of helicases into cellular processes. Q. Rev. Biophys. *36*, 1–69.

Dombroski, A.J., Brennan, C.A., Spear, P., and Platt, T. (1988). Site-directed alterations in the ATP-binding domain of rho protein affect its activities as a termination factor. J. Biol. Chem. *263*, 18802–18809.

Engel, D., and Richardson, J.P. (1984). Conformational alterations of transcription termination protein rho induced by ATP and by RNA. Nucleic Acids Res. *12*, 7389–7400.

Gai, D., Zhao, R., Li, D., Finkielstein, C.V., and Chen, X.S. (2004). Mechanisms of conformational change for a replicative hexameric helicase of SV40 large tumor antigen. Cell *119*, 47–60.

Galluppi, G.R., and Richardson, J.P. (1980). ATP-induced changes in the binding of RNA synthesis termination protein Rho to RNA. J. Mol. Biol. *138*, 513–539.

Geiselmann, J., and von Hippel, P.H. (1992). Functional interactions of ligand cofactors with Escherichia coli transcription termination factor rho. I. Binding of ATP. Protein Sci. *1*, 850–860.

Geiselmann, J., Seifried, S.E., Yager, T.D., Liang, C., and von Hippel, P.H. (1992a). Physical properties of the Escherichia coli transcription termination factor rho. 2. Quaternary structure of the rho hexamer. Biochemistry *31*, 121–132.

Geiselmann, J., Yager, T.D., Gill, S.C., Calmettes, P., and von Hippel, P.H. (1992b). Physical properties of the Escherichia coli transcription termination factor rho. 1. Association states and geometry of the rho hexamer. Biochemistry *31*, 111–121.

Geiselmann, J., Wang, Y., Seifried, S.E., and von Hippel, P.H. (1993). A physical model for the translocation and helicase activities of Escherichia coli transcription termination protein Rho. Proc. Natl. Acad. Sci. USA *90*, 7754–7758.

Gogol, E.P., Seifried, S.E., and von Hippel, P.H. (1991). Structure and assembly of the Escherichia coli transcription termination factor rho and its interaction with RNA. I. Cryoelectron microscopic studies. J. Mol. Biol. *221*, 1127–1138.

Hingorani, M.M., and Patel, S.S. (1993). Interactions of bacteriophage T7 DNA primase/helicase protein with single-stranded and double-stranded DNAs. Biochemistry *32*, 12478–12487.

Hingorani, M.M., Washington, M.T., Moore, K.C., and Patel, S.S. (1997). The dTTPase mechanism of T7 DNA helicase resembles the binding change mechanism of the F1-ATPase. Proc. Natl. Acad. Sci. USA *94*, 5012–5017.

Holton, J., and Alber, T. (2004). Automated protein crystal structure determination using ELVES. Proc. Natl. Acad. Sci. USA *101*, 1537–1542.

Horiguchi, T., Miwa, Y., and Shigesada, K. (1997). The quaternary geometry of transcription termination factor rho: assignment by chemical cross-linking. J. Mol. Biol. *269*, 514–528.

Iyer, L.M., Leipe, D.D., Koonin, E.V., and Aravind, L. (2004). Evolutionary history and higher order classification of AAA+ ATPases. J. Struct. Biol. *146*, 11–31.

Jeong, Y.J., Kim, D.E., and Patel, S.S. (2004). Nucleotide binding induces conformational changes in Escherichia coli transcription termination factor Rho. J. Biol. Chem. *279*, 18370–18376.

Jezewska, M.J., Kim, U.S., and Bujalowski, W. (1996). Binding of Escherichia coli primary replicative helicase DnaB protein to single-stranded DNA. Long-range allosteric conformational changes within the protein hexamer. Biochemistry *35*, 2129–2145.

Jones, T.A., Zou, J.Y., Cowan, S.W., and Kjeldgaard. (1991). Improved methods for building protein models in electron density maps and the location of errors in these models. Acta Crystallogr. A *47*, 110–119.

Kim, D.E., and Patel, S.S. (1999). The mechanism of ATP hydrolysis at the noncatalytic sites of the transcription termination factor Rho. J. Biol. Chem. *274*, 32667–32671.

Kim, D.E., and Patel, S.S. (2001). The kinetic pathway of RNA binding to the Escherichia coli transcription termination factor Rho. J. Biol. Chem. *276*, 13902–13910.

Lisal, J., and Tuma, R. (2005). Cooperative mechanism of RNA packaging motor. J. Biol. Chem. *280*, 23157–23164.

MacDowell, A.A., Celestre, R.S., Howells, M., McKinney, W., Krupnick, J., Cambie, D., Domning, E.E., Duarte, R.M., Kelez, N., Plate, D.W., et al. (2004). Suite of three protein crystallography beamlines with single superconducting bend magnet as the source. J. Synchrotron Radiat. *11*, 447–455.

Mancini, E.J., Kainov, D.E., Grimes, J.M., Tuma, R., Bamford, D.H., and Stuart, D.I. (2004). Atomic snapshots of an RNA packaging motor

reveal conformational changes linking ATP hydrolysis to RNA translocation. Cell *118*, 743–755.

McCoy, A.J., Grosse-Kunstleve, R.W., Storoni, L.C., and Read, R.J. (2005). Likelihood-enhanced fast translation functions. Acta Crystallogr. D Biol. Crystallogr. *61*, 458–464.

McSwiggen, J.A., Bear, D.G., and von Hippel, P.H. (1988). Interactions of Escherichia coli transcription termination factor rho with RNA. I. Binding stoichiometries and free energies. J. Mol. Biol. *199*, 609–622.

Miwa, Y., Horiguchi, T., and Shigesada, K. (1995). Structural and functional dissections of transcription termination factor rho by random mutagenesis. J. Mol. Biol. *254*, 815–837.

Modrak, D., and Richardson, J.P. (1994). The RNA-binding domain of transcription termination factor rho: isolation, characterization, and determination of sequence limits. Biochemistry *33*, 8292–8299.

Morgan, W.D., Bear, D.G., Litchman, B.L., and von Hippel, P.H. (1985). RNA sequence and secondary structure requirements for rho-dependent transcription termination. Nucleic Acids Res. *13*, 3739–3754.

Murshudov, G.N., Vagin, A.A., and Dodson, E.J. (1997). Refinement of macromolecular structures by the maximum-likelihood method. Acta Crystallogr. D Biol. Crystallogr. *53*, 240–255.

Noji, H., Yasuda, R., Yoshida, M., and Kinosita, K., Jr. (1997). Direct observation of the rotation of F1-ATPase. Nature *386*, 299–302.

Patel, S.S., and Picha, K.M. (2000). Structure and function of hexameric helicases. Annu. Rev. Biochem. *69*, 651–697.

Richardson, J.P. (1982). Activation of rho protein ATPase requires simultaneous interaction at two kinds of nucleic acid-binding sites. J. Biol. Chem. *257*, 5760–5766.

Richardson, J.P. (1996). Structural organization of transcription termination factor Rho. J. Biol. Chem. *271*, 1251–1254.

Richardson, J.P. (2002). Rho-dependent termination and ATPases in transcript termination. Biochim. Biophys. Acta *1577*, 251–260.

Richardson, J.P., and Conaway, R. (1980). Ribonucleic acid release activity of transcription termination protein rho is dependent on the hydrolysis of nucleoside triphosphates. Biochemistry *19*, 4293–4299.

Richardson, J.P., and Ruteshouser, E.C. (1986). rho factor-dependent transcription termination. Interference by a mutant rho. J. Mol. Biol. *189*, 413–419.

Sawaya, M.R., Guo, S., Tabor, S., Richardson, C.C., and Ellenberger, T. (1999). Crystal structure of the helicase domain from the replicative helicase-primase of bacteriophage T7. Cell *99*, 167–177.

Seifried, S.E., Bjornson, K.P., and von Hippel, P.H. (1991). Structure and assembly of the Escherichia coli transcription termination factor rho and its interactions with RNA. II. Physical chemical studies. J. Mol. Biol. *221*, 1139–1151.

Seifried, S.E., Easton, J.B., and von Hippel, P.H. (1992). ATPase activity of transcription-termination factor rho: functional dimer model. Proc. Natl. Acad. Sci. USA *89*, 10454–10458.

Shigesada, K., and Wu, C.W. (1980). Studies of RNA release reaction catalyzed by E. coli transcription termination factor rho using isolated ternary transcription complexes. Nucleic Acids Res. *8*, 3355–3369.

Singleton, M.R., Sawaya, M.R., Ellenberger, T., and Wigley, D.B. (2000). Crystal structure of T7 gene 4 ring helicase indicates a mechanism for sequential hydrolysis of nucleotides. Cell *101*, 589–600.

Singleton, M.R., Dillingham, M.S., Gaudier, M., Kowalczykowski, S.C., and Wigley, D.B. (2004). Crystal structure of RecBCD enzyme reveals a machine for processing DNA breaks. Nature *432*, 187–193.

Skordalakes, E., and Berger, J.M. (2003). Structure of the Rho transcription terminator: mechanism of mRNA recognition and helicase loading. Cell *114*, 135–146.

Stitt, B.L. (2001). Escherichia coli transcription termination factor Rho binds and hydrolyzes ATP using a single class of three sites. Biochemistry *40*, 2276–2281.

Stitt, B.L., and Xu, Y. (1998). Sequential hydrolysis of ATP molecules bound in interacting catalytic sites of Escherichia coli transcription termination protein Rho. J. Biol. Chem. *273*, 26477–26486.

von Hippel, P.H., and Delagoutte, E. (2001). A general model for nucleic acid helicases and their "coupling" within macromolecular machines. Cell *104*, 177–190.

Wang, J. (2004). Nucleotide-dependent domain motions within rings of the RecA/AAA(+) superfamily. J. Struct. Biol. *148*, 259–267.

Wei, R.R., and Richardson, J.P. (2001). Identification of an RNA-binding site in the ATP binding domain of Escherichia coli Rho by H2O2/Fe-EDTA cleavage protection studies. J. Biol. Chem. *276*, 28380–28387.

Xu, Y., Kohn, H., and Widger, W.R. (2002). Mutations in the rho transcription termination factor that affect RNA tracking. J. Biol. Chem. *277*, 30023–30030.

Xu, Y., Johnson, J., Kohn, H., and Widger, W.R. (2003). ATP binding to Rho transcription termination factor. Mutant F355W ATP-induced fluorescence quenching reveals dynamic ATP binding. J. Biol. Chem. *278*, 13719–13727.

Yu, X., Hingorani, M.M., Patel, S.S., and Egelman, E.H. (1996). DNA is bound within the central hole to one or two of the six subunits of the T7 DNA helicase. Nat. Struct. Biol. *3*, 740–743.

Yu, X., Horiguchi, T., Shigesada, K., and Egelman, E.H. (2000). Three-dimensional reconstruction of transcription termination factor rho: orientation of the N-terminal domain and visualization of an RNA-binding site. J. Mol. Biol. *299*, 1279–1287.

Accession Numbers

Coordinates for the structures described herein have been deposited in the RCSB Protein Data Bank with the ID code 2HT1.